AN ABSTRACT OF THE THESIS OF

Kenneth Robert Bitting (Name) for the Master of Science (Degree)

in Mechanical Engineering (Major) presented on October 26, 1972 (Date)

Title: A PHOTOELASTIC ANALYSIS OF A BEAM UNDER SHEAR AND COMPRESSIVE LOADS

Redacted for Privacy

Abstract approved: Dr. Hans J. Dahlke

The determination of failure is complicated when a structural element is subjected to combined rather than simple stresses. This is especially true when the principle of superposition does not apply. For such cases, tests of the element under the expected loads are required to determine its failure criteria.

In this investigation, a rectangular beam is subjected to combined shear and axial loads and studied experimentally. It is the object of this investigation to determine the effect of the axial compression on the maximum stresses created by the shear load. As a preliminary objective, the stress distribution along the shear plane will be determined using photoelastic techniques.

The distortion energy theory of failure, and its corollary the octahedral shear stress theory, establish a relationship between the combined applied loads and the yield stress of the material and will be

used in this investigation.

The distortion energy theory shows that, as axial compression increases, the distortion energy (and octahedral shear stress) increases indicating that the beam is approaching failure along the shear plane.

The normal stress distributions at the shear plane were determined and the effect of axial compression established. The shear stress was found to be a maximum near the edges of the beam. Under axial compression the shear stresses near the edges were reduced and the minimum stresses (at the midsection) were increased somewhat.

The normal stresses perpendicular to the plane of investigation were found to be compressive near the edges and tensile in the midsection. Axial compression is superimposed on the original profile, thereby increasing the stresses uniformly over the entire cross section.

The normal stresses parallel to the shear plane are of the same general shape and magnitude as the shear stress and are effected only under high axial compressive loads, probably due to the poisson effect.

A Photoelastic Stress Analysis of a Beam Under Shear and Compressive Loads

by

Kenneth Robert Bitting

A THESIS

submitted to

Oregon State University

in partial fulfillment of
the requirements for the
degree of

Master of Science

June 1973

APPROVED:

Redacted for Privacy

Associate Professor of Mechanical Engineering

in charge of major

Redacted for Privacy

Head of Department of Mechanical and Nuclear Engineering

Redacted for Privacy

Dean of Graduate School

Date thesis is presented October 26, 1972

Typed by Barbara Eby for Kenneth Robert Bitting

ACKNOWLEDGEMENTS

The author wishes to gratefully acknowledge the advice and assistance offered by his Major Professor, Dr. Hans J. Dahlke in the course of the research here reported.

A debt of gratitude is due also to the many graduate students and faculty members who gave freely and spontaneously of their time and assistance, and to the Weyerhaeuser Company for their financial support of this research project.

TABLE OF CONTENTS

LIST OF FIGURES

LIST OF TABLES

A PHOTOELASTIC STRESS ANALYSIS OF A BEAM UNDER SHEAR AND COMPRESSIVE LOADS

I. INTRODUCTION

The determination of the ultimate strength of a structural member requires a knowledge of the stress distribution and the physical properties of the material. From these the ultimate load can be evaluated utilizing a suitable failure theory as a criteria.

For most ductile materials, failure is considered to occur when the material begins to yield. At and beyond the yield point, strain is no longer linearly proportional to stress and a specimen will be permanently deformed after the load is removed.

For a brittle material, fracture constitutes failure. In either case, failure is that point at which the material first deviates from the elastic stress-strain relationship.

The analysis of failure is complicated when the structural element is subjected to combined rather than simple stresses. This is especially true when the principle of superposition does not apply as is the case when a beam is subjected to bending and torsion. For such cases, tests of the element under the expected loads are required to determine its failure criteria.

Another way of estimating the failure of a structural element is by simulating its load conditions with a model and analyzing the model.

Such a procedure will be reported in this investigation. A rectangular beam subjected to a combined shear and axial load (Figure 1) is studied experimentally. It is the object of this investigation to determine the effect of the axial compression (F_c) on the maximum stresses created by the shear load (F_s) at the shear plane, section A-A, Figure 1.

As a preliminary objective, the stress distribution along the plane of interest will be determined experimentally using photoelastic techniques. The photoelastic analysis, combined with a numerical integration of the equations of equilibrium, gives the normal and shear stresses at selected points along the plane.

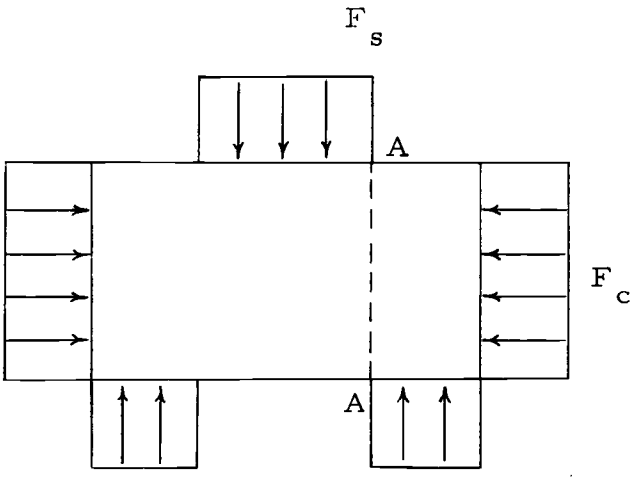

Figure 1. Load schematic diagram.

The distortion energy theory of failure, and its corollary, the octahedral shear stress theory, establishes a relationship between the combined applied loads and the yield stress of a material. It will be used in this investigation.

One way of determining the stress distribution theoretically consists of finding a stress function which satifies the boundary conditions. In this case, an exact mathematical solution is precluded by the fact that the load is discontinuous at the point of interest resulting in a discontinuity in the boundary conditions. Durant and Garwood (3) found it impossible to derive a stress function which satisfied all necessary boundary conditions.

A literature survey shows that little experimental or theoretical work has been performed on the load configuration with which this investigation concerns itself. A discussion of similar investigations, however, will serve as an introduction to the topic and provide valuable background information and insight for this analysis.

In an attempt to analytically determine the stresses along section A-A, Figure 1, Inglis (1, p. 607) approximated the problem by deriving a stress function involving a Fourier series for the area immediately around the shear plane. Two cases are considered; first, the plate ABCD (Figure 2a) has its edges AB and CD absolutely fixed, while the two edges AD and BC are subjected to uniformly distributed shear, and second, the plate ABCD is subjected to shear uniformly

distributed along all four edges.

If the stress functions for these cases are combined and made to satisfy the displacement condition of the boundaries, the edges AD and BC can be freed from shear and a close approximation to the analytical case is obtained.

Inglis found that the shear stress was a maximum near the edges of the beam and decreased somewhat in the central portion.

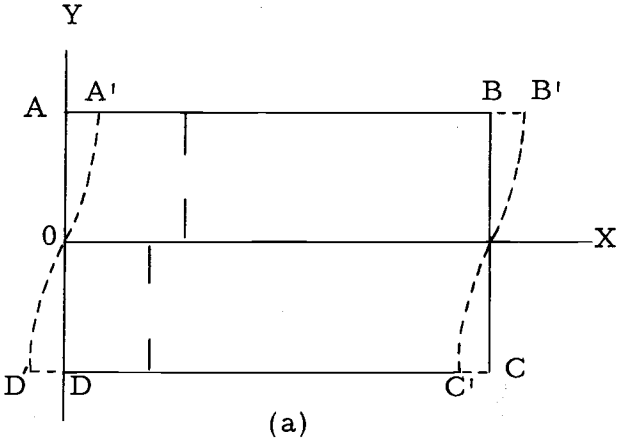

(a)

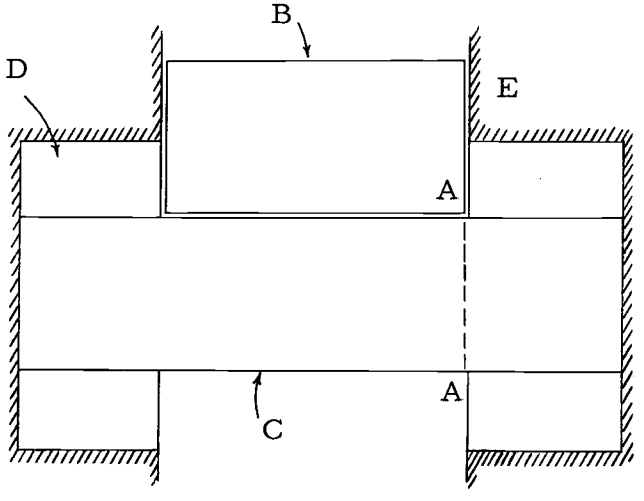

(b)

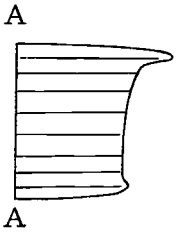

Shear stress distribution at section A-A

(c)

Figure 2. Ingus and Fukuda investigations.

Fukuda reached the same conclusion experimentally (1, p. 611). In his photoelastic analysis, a transparent beam C (Figure 2b) of rectangular cross section is supported by block D of the same material in a rigid frame E. The load is applied through block B. The use of the same material in supporting the beam and applying the load was found by this author to be a significant factor in distributing the load properly and obtaining an accurate stress pattern. The stress trajectories (which are curves the tangent to which represents the directions of one of the principal stresses at the points of tangency) indicate that the stress distribution at section A-A is not one of pure shear because they do not intersect the section A-A at an angle of 45^{o}. The shear stress (Figure 2c) across section A-A is seen to be at a maximum near the top of the beam. Such a stress profile is typical of this load configuration and will be encountered frequently in the chapters to follow.

J. N. Goodier (9) developed an analytical solution for the stress perpendicular to the line of force in a block compressed on opposite sides by a concentrated force (Figure 3a). He showed that the normal stress (Figure 3b) is compressive near the load points but becomes tensile in the central portion of the beam. Since assigning the proper arithmetic signs to the terms of the shear difference equation (Equation 22a) is critical, this observation is valuable since it gives an indication of what form the stress profile should take.

In a paper presented to the Royal Society of London, L. N. G. Filon (7) derived an expression for the shear stress distribution for a beam loaded as shown in Figure 4a. He not only verified the results of previous investigations (Inglis, Fukuda) (Figure 4b), but he also showed that the shear stress distribution across the shear plane under consideration is a function of the distance between the load points (the distance 2ℓ in Figure 4a). This is an important point to note when performing a series of analyses, particularly on beams of different depths. The effect of varying the load and beam dimensions on the stress profile will not be masked by a variation in the load point separation (2ℓ) if the ratio of the depth to the load point separation is kept constant in all trials.

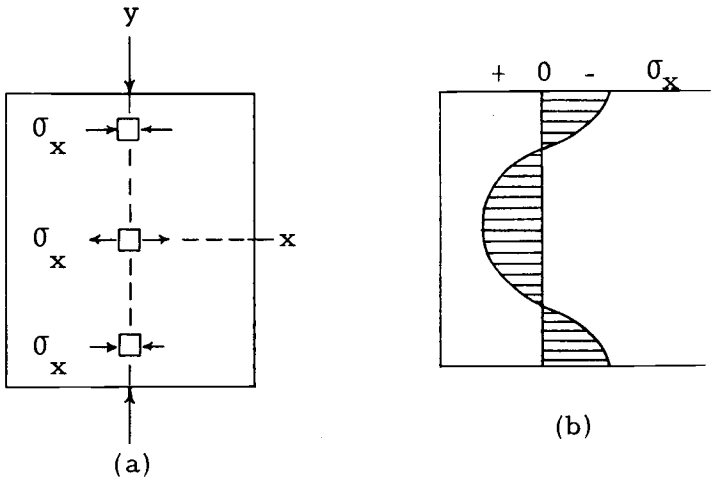

Figure 3. Concentrated force on block.

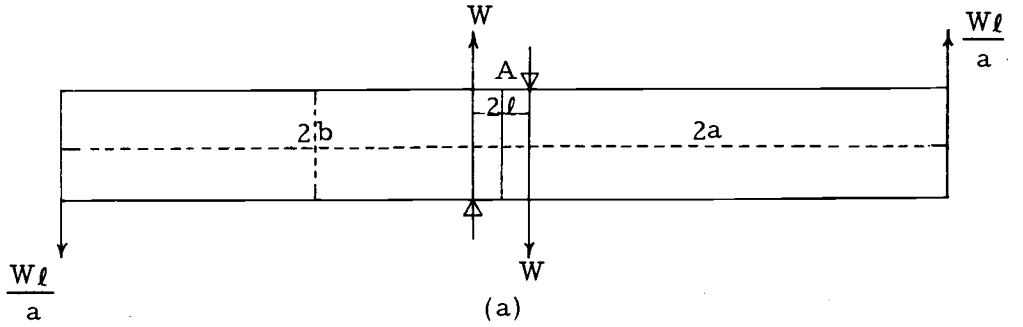

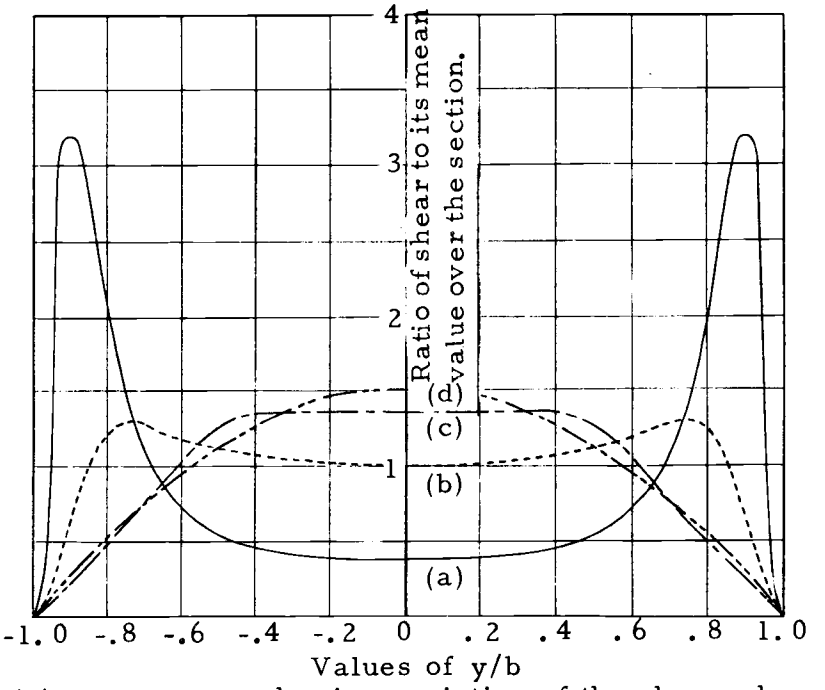

(a) ——— curve showing variation of the shear when $\ell = .1b$
(b) ------- curve showing variation of the shear when $\ell = .35b$
(c) —·— curve showing variation of the shear when $\ell = .52b$
(d) —··— curve showing variation of the shear when $\ell = \infty$

Figure 4. Concentrated force not symmetrical.

II. ENERGY OF DISTORTION THEORY

Total Strain Energy

The total elastic strain energy per unit volume (W_t) at a point in a stressed element involves both the stress and strain at the point in question and can be expressed in terms of principal strains and stresses as

$$W_t = \frac{1}{2}\sigma_1\epsilon_1 + \frac{1}{2}\sigma_2\epsilon_2 + \frac{1}{2}\sigma_3\epsilon_3 \tag{1}$$

The principal strains ϵ_1, ϵ_2, ϵ_3 are related to the principal stresses σ_1, σ_2 and σ_3 through Hooke's law as follows:

$$\begin{aligned}
\epsilon_1 &= \frac{\sigma_1}{E} - \mu\frac{\sigma_2}{E} - \mu\frac{\sigma_3}{E} \\
\epsilon_2 &= \frac{\sigma_2}{E} - \mu\frac{\sigma_1}{E} - \mu\frac{\sigma_3}{E} \\
\epsilon_3 &= \frac{\sigma_3}{E} - \mu\frac{\sigma_1}{E} - \mu\frac{\sigma_2}{E}
\end{aligned} \tag{2}$$

Substituting Equations (2) into Equation (1), W_t can be expressed in terms of the principal stresses only.

$$W_t = \frac{1}{2E}[\sigma_1^2 + \sigma_2^2 + \sigma_3^2 - 2\mu(\sigma_1\sigma_2 + \sigma_2\sigma_3 + \sigma_1\sigma_3)] \tag{3}$$

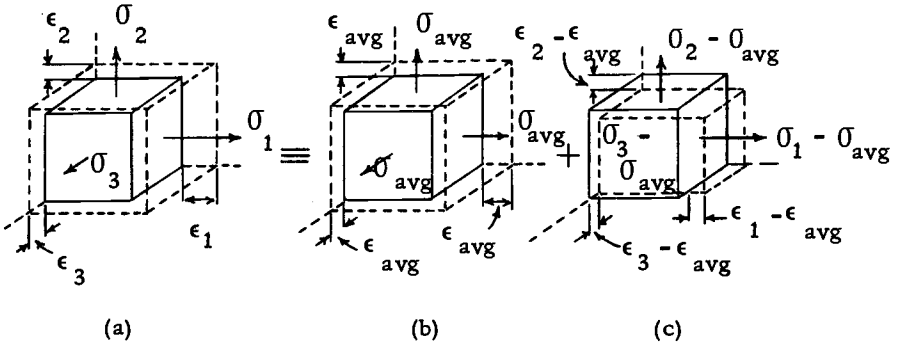

Figure 5. Component stress system.

Distortion Energy

Von Mises and Hencky (13) proposed that the total strain energy be resolved into two parts; first, the strain energy of uniform tension or compression (that associated with the change in volume of the unit volume) and second, the strain energy of distortion or change of shape. They proposed that the energy absorbed in changing the volume in an ideal material has no effect in causing failure by yielding, and that failure by inelastic action is associated with the energy absorbed in changing shape.

To resolve the total strain energy into these two parts, the principal stresses (Figure 5) are resolved into two component states of stress (Figure 5b and c) such that in one of the component states the average of the principal stresses, σ_{ave}, act on the three faces of the unit volume (Figure 5b) and produce strains equal to the average

of the three principal strains, ϵ_{ave}. The second component state as shown in Figure 5c consists of the remainder of each of the three principal stresses.

The average principal stress, σ_{ave}, produces the entire volume change (ϵ_v) of the unit cube. The remaining components of the three principal stresses (Figure 5c) do not produce a volume change since the sum of the three strains in Figure 5c is zero. These stresses do distort the cube and a change of shape occurs. The sum of the strain energies produced by the two component states of Figure 5b and c is equal to the total strain energy, W_t. Therefore,

$$W_t = W_v + W_d \tag{4}$$

where W_v is the energy of volume change per unit volume and W_d is the distortion energy per unit volume.

W_v can be computed from the stresses and strains shown in Figure 5b and is given by

$$W_v = \frac{1}{2}\sigma_{ave}\epsilon_{ave} + \frac{1}{2}\sigma_{ave}\epsilon_{ave} + \frac{1}{2}\sigma_{ave}\epsilon_{ave} = \frac{1}{2}\sigma_{ave}\epsilon_v . \tag{5}$$

Since

$$\epsilon_v = \frac{\sigma_{ave}}{E_v}$$

Equation (5) becomes

$$W_v = \frac{(\sigma_{ave})^2}{2E_v} \quad , \quad \text{where } \sigma_{ave} = \frac{\sigma_1 + \sigma_2 + \sigma_3}{3} \text{ and } E_v = \frac{E}{3(1-2\mu)}$$

From Equation (4), the energy of distortion can be determined by subtracting the energy of volume change from the total strain energy. Thus

$$W_d = W_t - W_v$$

$$= \frac{1}{2}E[\sigma_1^2 + \sigma_2^2 + \sigma_3^2 - 2\mu(\sigma_1\sigma_2 + \sigma_2\sigma_3 + \sigma_1\sigma_3] - \frac{(\sigma_{ave})^2}{2E_v} .$$

This reduces to

$$W_d = \frac{1+\mu}{6E}[(\sigma_1 - \sigma_2)^2 + (\sigma_2 - \sigma_3)^2 + (\sigma_1 - \sigma_3)^2] \qquad (6)$$

Distortion Energy of Failure Theory

Equation (6) is the basis for determining failure of ductile materials having a pronounced yield point stress, σ_{yp}, in simple tension. The distortion energy theory of failure states that yielding begins when the distortion energy reaches a maximum and equals the value of the distortion energy at the yield point in a simple tensile test. Therefore, letting

$$\sigma_1 = \sigma_{yp} \qquad \sigma_2 = \sigma_3 = 0$$

Equation (6) becomes

$$W_d = \frac{(1+\mu)}{3E}\sigma_{yp}^2 .$$

This is the value of W_d at which yielding occurs.

Octahedral Shear Stress Theory

A corollary to the distortion energy theory is the octahedral shear stress theory. This theory will be employed here because it is in familiar terms of stress rather than energy terms.

The same condition for yielding may be obtained by considering the shear stress acting on an octahedral plane (15) such as ABC in Figure 6. The unit volume in Figure 6 is acted upon by the principal

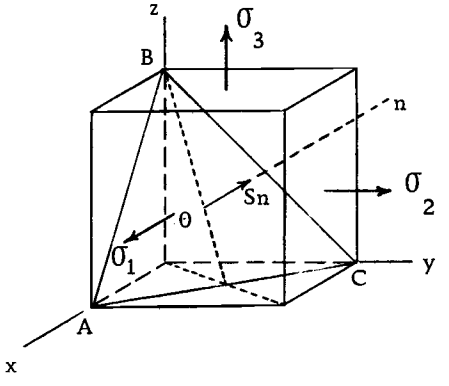

Figure 6. Octahedral element.

stresses σ_1, σ_2 and σ_3. Resolving the unit stress S acting on the octahedral plane into three components S_x, S_y and S_z and knowing that the cosine of the angle between the normal to the octahedral plane and the coordinate axis is $\frac{1}{\sqrt{3}}$, it is found that

$$S_x = \frac{\sigma_1}{\sqrt{3}} \qquad S_y = \frac{\sigma_2}{\sqrt{3}} \qquad S_z = \frac{\sigma_3}{\sqrt{3}} \quad .$$

The resultant unit stress S acting on the octahedral plane is then

$$S = \sqrt{S_x^2 + S_y^2 + S_z^2}$$

$$= \frac{1}{\sqrt{3}} \sqrt{\sigma_1^2 + \sigma_2^2 + \sigma_3^2} \quad .$$

The normal component S_n of the stress S is obtained by projecting S_x, S_y and S_z in the direction of the normal, n,

$$S_n = \frac{\sigma_1 + \sigma_2 + \sigma_3}{3}$$

The shear stress τ_{oct} on the octahedral plane is then given by

$$\tau_{oct} = \sqrt{S^2 - S_n^2}$$

$$= \frac{1}{3} \sqrt{(\sigma_1 - \sigma_2)^2 + (\sigma_2 - \sigma_3)^2 + (\sigma_1 - \sigma_3)^2}. \qquad (7)$$

The octahedral shear stress can be expressed in terms of the energy of distortion in Equation (6) by multiplying and dividing the right side of Equation (7) by $\sqrt{\frac{1+\mu}{6E}}$. Thus

$$\tau_{oct} = \frac{1}{3} \sqrt{\frac{6E}{1+\mu}} \sqrt{\frac{1+\mu}{6E} [(\sigma_1 - \sigma_2)^2 + (\sigma_2 - \sigma_3)^2 + (\sigma_1 - \sigma_3)^2]}$$

(8)

Referring to Equation (6), Equation (8) becomes

$$\tau_{oct} = \frac{1}{3}\sqrt{\frac{6EW_d}{1+\mu}}$$

According to the energy of distortion theory, the failure criterion states that inelastic action begins when W_d reaches a maximum and $W_d = \frac{(1+\mu)\sigma_{yp}^2}{3E}$. Therefore, Equation (7) becomes

$$\tau_{oct} = \frac{\sqrt{2}}{3}\sigma_{yp} = .47\,\sigma_{yp} .$$

The octahedral shear stress theory states that inelastic action at any point in a body subjected to any combination of stresses begins only when the octahedral shear stress becomes equal to the octahedral shear stress at the yield point in a simple tensile test.

The failure criteria of a point in a body can be displayed in a plot of Equation (7) which is an ellipse (Figure 7). The ellipse represents the combination of principal stresses at which failure will occur. In a specimen stressed below the elastic limit of the material, the stresses at all points within the body fall within the ellipse. As the load is increased and failure approaches, the points move toward the boundary.

The octahedral shear stress distribution at all points on a cross section may be displayed in a continuous curve which has the ratio of the coordinate distance Y to the depth of the model D on the abscissa, and the octahedral shear stress on the ordinate. As the load increases,

the curve is displayed in the direction of increasing octahedral shear stress indicating that the specimen is approaching failure.

The distortion energy theory has been found to agree very well with experimental results and seems to combine the best points of the various failure theories.

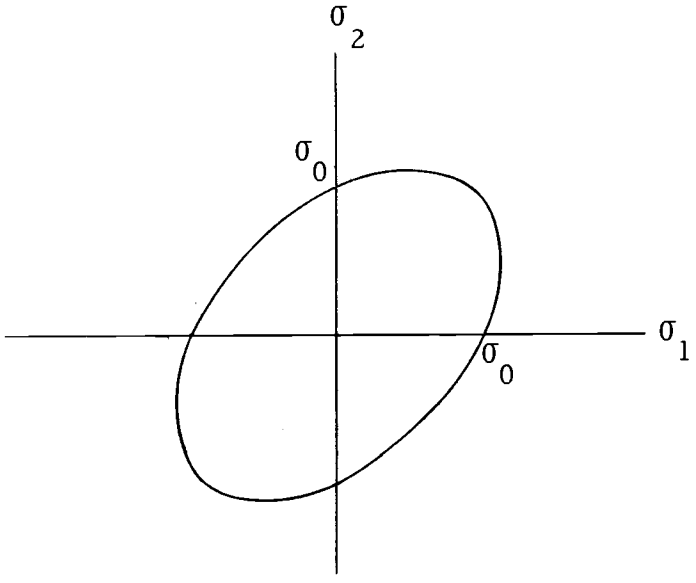

Figure 7. Distortion energy theory failure criteria.

Orthotropic Materials

The distortion energy theory as presented thus far applies to isotropic materials exclusively. Norris (12) extended this theory to orthotropic materials (e. g. wood, fiber glass laminations) in the following manner.

Equation (6) expressed in terms of normal and shear stresses becomes

$$W_d = \frac{1}{12G}[(\sigma_x - \sigma_y)^2 + (\sigma_y - \sigma_z)^2 + (\sigma_x - \sigma_z)^2] + \frac{1}{2G}[\tau_{xy}^2 + \tau_{zy}^2 + \tau_{xz}^2] \tag{9}$$

where

$$G = \frac{E}{2(1+\mu)}$$

An orthotropic material is considered to be made up of an isotropic material with equally spaced rectangular voids. The walls of isotropic material between these voids are parallel to the x, y, and z axes so that these represent the natural axes of the orthotropic material.

If the walls of an element are subjected to a two-dimensional stress system, Equation (9) becomes

$$W_d = \frac{1}{6G}[\sigma_x^2 - \sigma_x\sigma_y + \sigma_y^2] + \frac{1}{2G}\tau_{xy}^2 .$$

If it is assumed that the stresses in the isotropic walls (σ) are proportional to the values of the stresses (f) applied to the orthotropic material,

$$\sigma_x = r_x f_x$$

$$\sigma_y = r_y f_y$$

$$T_{xy} = r_{xy} f_{xy} .$$

Substituting these values into Equation (9) yields

$$W_d = \frac{1}{6E}\left[r_x^2 f_x^2 - r_x f_x r_y f_y + r_y^2 f_y^2\right] + \frac{1}{2G} r_{xy}^2 f_{xy}^2 \quad . \qquad (10)$$

If a specimen is caused to fail in a uniaxial state of stress,

$$W_d = \frac{r_x^2 F_x^2}{6G}$$

where F_x denotes the stress at failure.

Solving the above equation for r_x gives

$$r_x = \frac{\sqrt{6GW_d}}{F_x} \quad .$$

Repeating this procedure for the other stresses, gives

$$r_y = \frac{\sqrt{6GW_d}}{F_y}$$

$$r_{xy} = \frac{\sqrt{2GW_d}}{F_{xy}} \quad .$$

When these values are substituted into Equation (1), the following equation is obtained

$$1 = \frac{f_x^2}{F_x^2} - \frac{f_x f_y}{F_x F_y} + \frac{f_y^2}{F_y^2} + \frac{f_{xy}^2}{F_{xy}^2} \qquad (11)$$

This is the distortion energy theory of failure as applied to an orthotropic material.

III. PHOTOELASTICITY

Certain transparent materials exhibit optical anisotropy when they are subjected to stress. This birefringence, or double refraction, forms the basis of the photoelastic technique of stress analysis.

Light traveling through an isotropic medium propagates with the same velocity in every direction (5). Light entering an anisotropic medium is divided or refracted into two plane-polarized components traveling with velocities that are inversely proportional to the index of refraction of their respective planes.

Let

n_1, n_2 = indices of refraction for the two principal directions of the plate.

v_1, v_2 = velocities of propagation of the components of light.

t_1, t_2 = times required for the component of light to travel through the plate.

n, v = index of refraction and velocity of propagation in the isotropic medium outside the plate.

c = velocity of light in a vaccum.

then

$$n_1 = \frac{c}{v_1} \qquad n_2 = \frac{c}{v_2} \qquad n = \frac{c}{v} \quad . \tag{12}$$

Substituting the following

$$v_1 = \frac{d}{t_1} \qquad v_2 = \frac{d}{t_2} \qquad v = \frac{d}{t}$$

into Equation (12) yields

$$n_1 = \frac{ct_1}{d} \qquad n_2 = \frac{ct_2}{d} \qquad n = \frac{ct}{d}$$

where t is the time required for the light to travel a distance d in the isotropic medium (outside the plate).

The phase angles of two waves with respect to the medium outside the birefringent material are

$$\alpha_1 = \omega(t_1 - t) = \frac{\omega d}{c}(n_1 - n) = \frac{2\pi d}{\lambda}(n_1 - n)$$

$$\alpha_2 = \omega(t_2 - t) = \frac{\omega d}{c}(n_2 - n) = \frac{2\pi d}{\lambda}(n_2 - n)$$

The angular phase difference is

$$\alpha = \alpha_1 - \alpha_2 = \frac{\pi 2d}{\lambda}(n_1 - n_2) \tag{13}$$

The linear phase difference is

$$\delta = \frac{\alpha\lambda}{2\pi} \tag{14}$$

where λ is the wavelength of light.

The linear phase difference is related to the wavelength and called the relative phase difference

$$R = \frac{\delta}{\lambda} \tag{15}$$

Combining Equations (13), (14) and (15) gives

$$R = \frac{d}{\lambda}(n_1 - n_2) \tag{16}$$

This relative linear phase difference is called the relative retardation and is proportional to the thickness of the plate, the difference in principal indices of refraction and inversely proportional to the wavelength of the light source.

Stress-Optic Law

It was found that the principal stresses are linearly related to the indices of refraction and that the difference in indices of refraction between the unstressed material n_o and the stressed material n_a, n_b and n_c bears a relationship to the principal stresses similar to that which exists between stress and strain.

Recalling the definition of strain and Hooke's law gives

$$\ell_1 - \ell_o = \ell_o \epsilon_1 = \frac{\ell_o}{E}\sigma_1 - \frac{\mu \ell_o}{E}(\sigma_2 + \sigma_3) .$$

Similarly, it was found that

$$n_a - n_o = C_1\sigma_1 - C_2(\sigma_2 + \sigma_3)$$

where C_1 and C_2 are stress-optical coefficients.

For a two-dimensional case,

$$\begin{aligned} n_a - n_o &= C_1\sigma_1 - C_2\sigma_2 \\ n_b - n_o &= C_1\sigma_2 - C_2\sigma_1 \end{aligned} \tag{17}$$

Equation (17) is the two-dimensional stress-optical law in terms of absolute retardation. Since the determination of absolute retardation is very time-consuming and delicate, most analyses make use of relative retardation.

Eliminating n_o from Equation (17),

$$n_a - n_b = (C_1 + C_2)(\sigma_1 - \sigma_2)$$

and substituting into Equation (17)

$$R = \frac{t}{\lambda}(n_a - n_b) = \frac{(C_1 + C_2)}{\lambda}(\sigma_1 - \sigma_2) .$$

Combining the stress-optic coefficients into one, we obtain

$$R = \frac{Ct}{\lambda}(\sigma_1 - \sigma_2) . \qquad (18)$$

Optics of the Polariscope

The plane polariscope consists of a light source, a polarizer and an analyzer. The polarizer and analyzer produce plane-polarized light; that is, they pass only light that vibrates in one particular plane.

When a stressed photoelastic model, made of a birefringent material, is placed between the polarizer and analyzer with one of its principal axes oriented at an angle θ with the horizontal, a light beam enters the plate and is resolved into two components (Figure 8):

$$A_1 = a \cos \theta \sin \omega t$$

$$A_2 = a \sin \theta \sin \omega t .$$

These components emerge with an angular phase difference α which is related to the indices of refraction, wavelength and plate thickness as given in Equation (13). The two emerging components are

$$A_3 = a \cos \theta \sin \omega t$$

$$A_4 = a \sin \theta \sin (\omega t + \alpha).$$

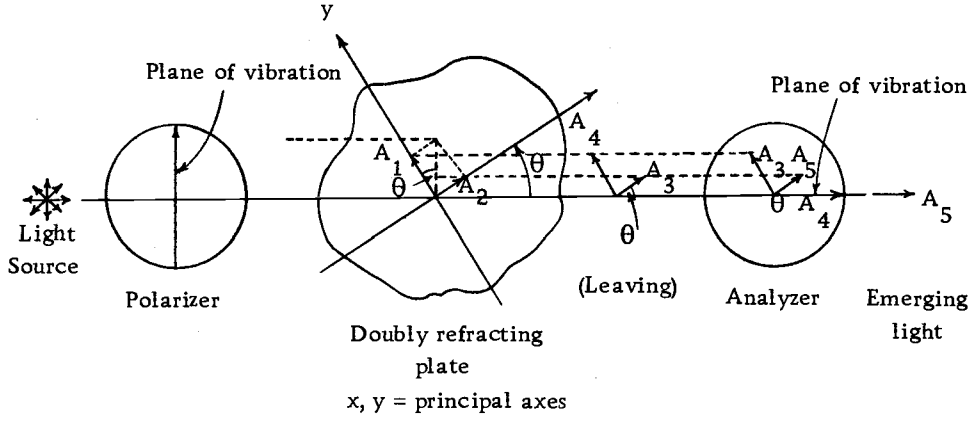

Figure 8. Optic of the polariscope.

If the plane of polarization of the polariscope is vertical and that of the analyzer is horizontal (the polarizer and analyzer are therefore crossed), then only the horizontal components of A_3 and A_4 will pass through the analyzer. The emerging beam is

$$A_5 = A_3 \cos \theta - A_4 \sin \theta$$

$$= b \cos (\omega t + \frac{\alpha}{2})$$

where $b = a \sin 2\theta \sin(\frac{\alpha}{2})$ is the amplitude.

The intensity of a light beam is taken as twice the square of the amplitude. Therefore

$$I = 2a^2 \sin^2 2\theta \sin^2 \frac{\alpha}{2} .$$

Light extinction occurs when the intensity is equal to zero. There are two possibilities;

(1) $$2\theta = n\pi$$

where n is an integer. Of special interest is

$$\theta = 0 \text{ or } \frac{\pi}{2} .$$

That is, one principal axis of the birefringent plate is parallel to the orientation plane (or vibration) of the polarizer and the other axis is perpendicular to the plane of vibration.

The other possibility for extinction is

(2) $$\frac{\alpha}{2} = n\pi$$

or, from Equations (14) and (15),

$$R = \frac{\alpha}{2\pi} = n \qquad (19)$$

which indicates that the relative retardation is an integral number of wavelengths.

Isochromatics

Viewing the photoelastic model through the analyzer of the polariscope (using monochromatic light), it is seen that fringes appear as the load is increased. These fringes represent consecutive integral values of relative retardation (Equation 14). Therefore, each fringe is said to have a fringe order which corresponds to its value of relative retardation. Figures 15 and 16 show examples of the fringe patterns developed at section A-A of Figure 1.

Returning to Equation (18), and considering what has been learned in Equation (19), Equation (18) can be written as

$$n = \frac{Ct}{\lambda}(\sigma_1 - \sigma_2) \tag{20}$$

where n is the fringe order.

From Equation (20), it can now be stated that every fringe of a given fringe order is a locus of points representing a constant principal stress difference $(\sigma_1 - \sigma_2)$.

Since

$$\tau_{max} = \frac{\sigma_1 - \sigma_2}{2}$$

Equation (20) becomes

$$\tau_{max} = \frac{n\lambda}{2Ct} = nF \tag{21}$$

where

$$F = \frac{\lambda}{2Ct}$$

is called the model fringe value measured in psi/fringe.

Isoclinics

As noted previously, there are two conditions which lead to the extinction of light, or the formation of fringes, in a photoelastic model. The first is due to the relative retardation (isochromatics). The second is associated with the angel θ between the reference axis and the principal stress axis. The fringes associated with this condition are referred to as the isoclinics. The isoclinic is the locus of all points where one principal stress is at an angle θ from the reference axis. This angle is the angle 2θ on Mohr's circle (Figure 19) and is therefore used in calculating the shear stress (Equation 25).

Since the intensity in a plane polariscope is a function of both the angle θ and the relative retardation or fringe order n, the isochromatic and isoclinic fringe patterns are superimposed on each other. This hinders the recording of photoelastic data since it may be difficult to distinguish between the two.

The isoclinics are eliminated in what is called the circular polariscope. This polariscope has quarter-wave plates on either side of the photoelastic model which retards the beam by one quarter of a wavelength. The principal axis of the quarter-wave plates are at 45^{o} angles to the horizontal axis. This causes the $\sin^{2}2\theta$ term in the intensity equation to always be equal to one. Thus the expression for the

intensity becomes

$$I = 2a^2 \sin^2 \frac{\alpha}{2}$$

and is related only to the relative retardation.

IV. APPARATUS

Loading Fixture

The photoelastic model to be analyzed is placed in a fixture capable of loading the model in shear and axial compression at two sections (Figure 1). Because the photoelastic process is a sensitive one, the fixture must be carefully designed to prevent alterations of the stress pattern in the model. Therefore, this fixture is designed with a maximum degree of flexibility to allow adjustments of the model in the fixture and the fixture in the polariscope. In this way, erroneous loads can be detected photoelastically and removed by adjustment.

For simplicity, the fixture was designed in two separate assemblies. The Shear Assembly applies the shear load by placing the model between two opposing members as shown in Figure 9. One end of the fixture is attached to a load cell in the loading frame of the polariscope to measure the total shear applied to the model. The other end of the fixture is attached to the movable end of the load frame. The load is applied at this end by moving the fixed and free ends of the frame apart, thereby placing the model in shear at section A-A, Figure 1. All joints in the shear assembly are pinned to relieve any bending moments caused by misalignment of the fixture. Figure 11 shows the fixture in the loading frame and Figure 12 shows the loading frame in the polariscope.

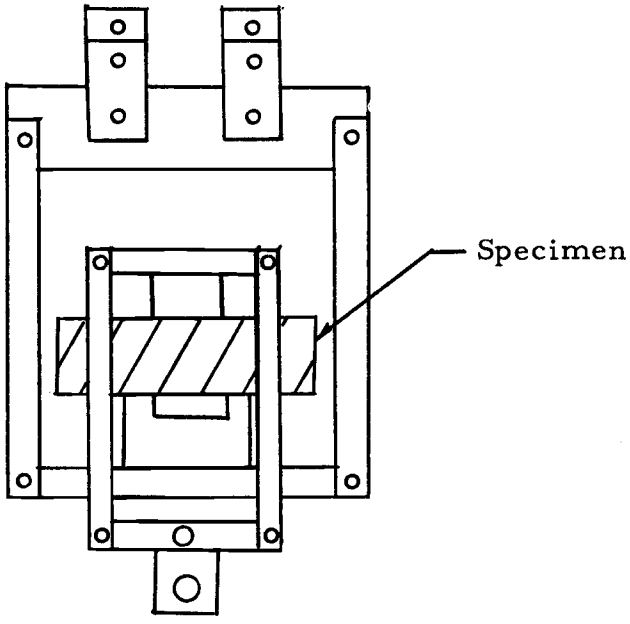

Figure 9. Shear assembly.

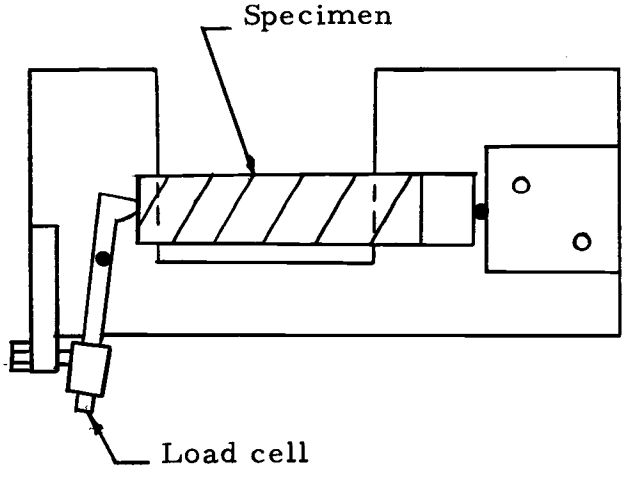

Figure 10. Compressive assembly.

Bearing pads made of the model material must be used between the aluminum surfaces of the fixture and the surfaces of the plastic model to reduce the high stress concentration between the dissimilar materials at section A-A near the edges of the model. This practice is in accordance with Coker and Filon and was discussed in Chapter I.

The model is subjected to axial compressive force by the Compressive Assembly shown in Figure 10. The compressive load is applied with and monitoredby a cantilever beam load cell. The load cell is composed of an aluminum beam with a strain gage mounted on the edges over the pivot hole. Placing the gages in this manner permits greater sensitivity because that is the point of maximum flexure. The strain gages are connected to adjacent arms (11, p. 7-5) of a Baldwin-Lima-Hamilton Strain Indicator. The load cell was calibrated using another load cell.

At high loads, the load cell travels through a relatively large arc. This causes the beam to rotate about the opposite end. A fulcrum is provided to facilitate this rotation and eliminate any bending moment which might develop if that end was fixed.

Axial compression is applied while the fixture is in the polariscope so any bending can be detected photoelastically and the appropriate adjustment made.

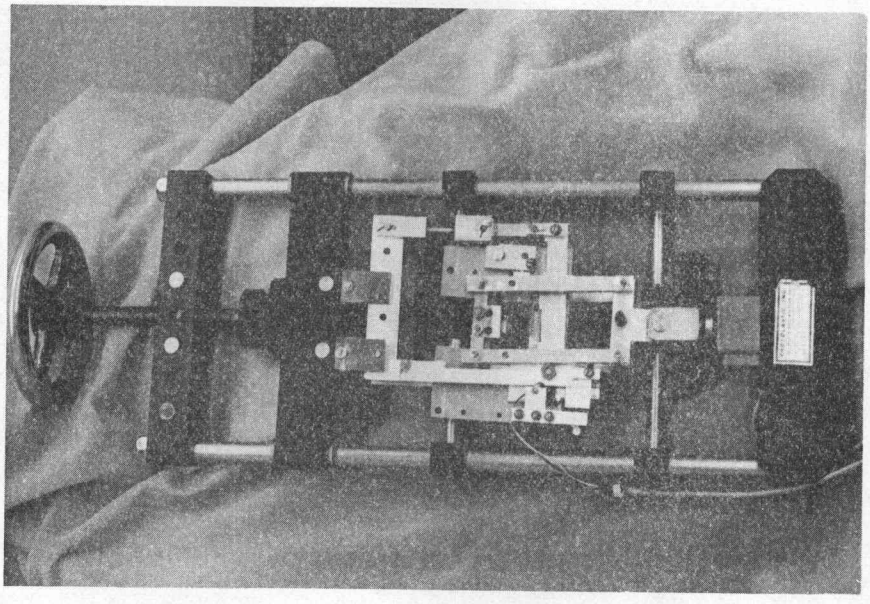

Figure 11. Fixture in loading frame.

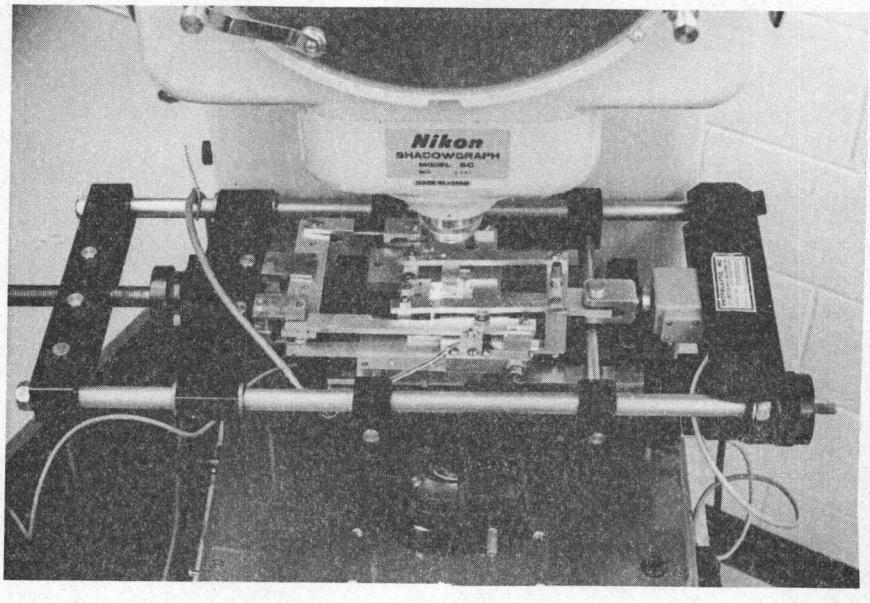

Figure 12. Fixture in polariscope.

Models

The three models used in the analysis are rectangular beams shaped from a quarter-inch sheet of Columbia Resin, CR-39, a thermosetting plastic. This material was selected because of optical clarity, freedom from residual stresses and availability.

With CR-39, a clear and colorless material, isoclinic and isochromatic patterns are not obscured. This is often the case when dark isoclinics and isochromatics blend with the dark color of translucent model materials. In this application, optical clarity is of major importance because isoclinics tend to wash out under compressive loads.

The disadvantage of using CR-39 is its optical creep, an increase of retardation which causes a gradual increase in the fringe order and therefore, a decrease in the stress-optic coefficient (8, vol. 1, p. 367).

It is assumed that optical creep affects the moduli of elasticity and rigidity in the same way so that the stress distribution (the isoclinics and isochromatics considered as a family of curves) remain unchanged (6, p. 86). Accordingly, the stress-optic coefficient must decrease to preserve a direct proportionality between the stress and the fringe order.

Figure 13 (5, p. 114) shows the variation of fringe order with time at different loads in CR-39. Two points should be noted. First,

the fringe order changes most rapidly shortly after the load is applied, and second, the higher the load the more appreciable the creep. These two points should be considered when deciding what loads to apply and when to record the data.

Because strain is proportional to stress only below 3000 psi in CR-39 (2, p. 79), a low load is necessary to reduce the effect of creep. A one-hour lapse between loading and recording data allows time-dependent effects of creep to dissipate.

The models were cut to their approximate dimensions on a jig-saw then machined to the final dimensions as shown in Figure 14. The edges must be polished with fine emery cloth to insure the removal of small surface discontinuities which often cause a drastic distortion of the fringe pattern.

The bearing pads mentioned previously must be machined and polished with the same care that is given to the model.

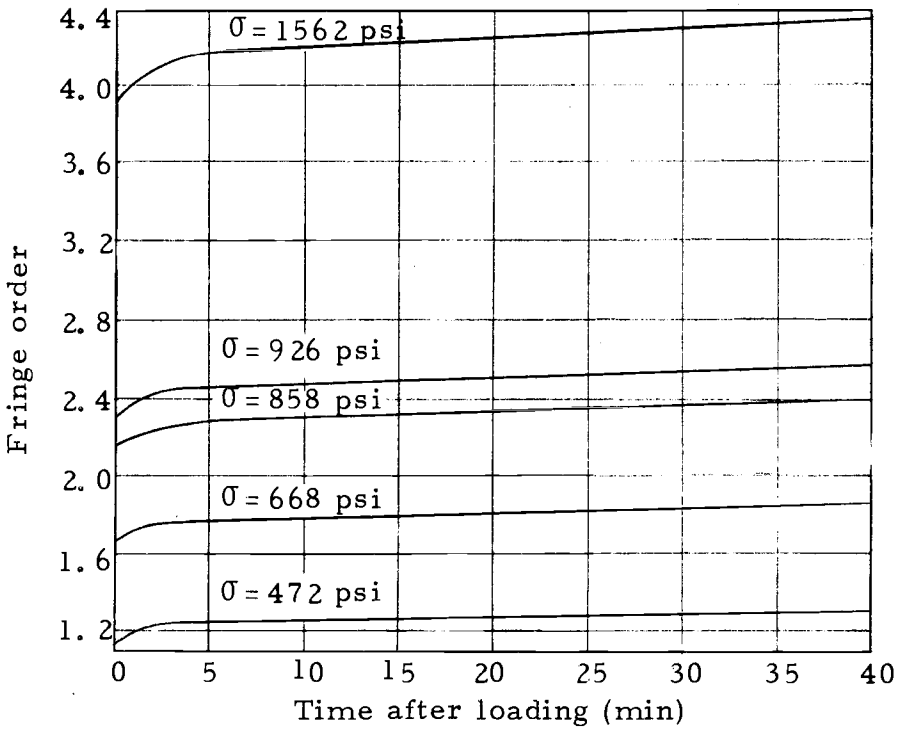

Figure 13. Optical creep in CR-39.

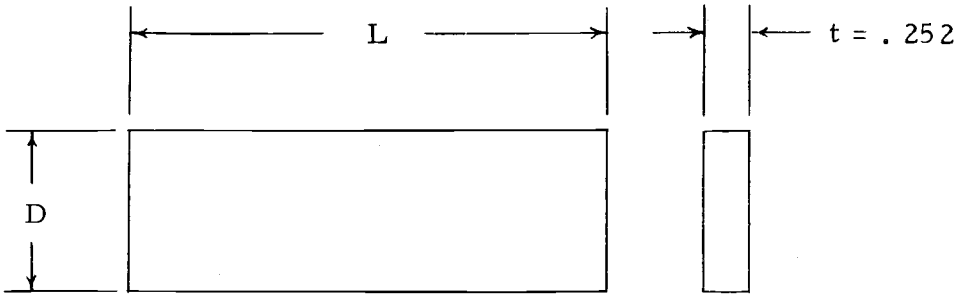

Trial	L	D
3	2.5	.252
4	2.5	.505
5	2.5	.749

Figure 14. Model dimensions.

V. RECORDING PHOTOELASTIC DATA

After sufficient experimentation, the forces in Table 1 were adopted for this experiment. The shear force F_v and the axial compressive force F_c are defined in Figure 1. The force ratio is equal to F_c/F_v and "LPS" is the load point separation (Figure 20). L/D is the length to depth ratio (Figure 14).

Since the shear plane thickness has a very definite effect on the stress distribution (Figure 4), the ratio of the load point separation to the model depth is held constant for all trials. This measurement was made directly on the polariscope screen which displays a model image ten times actual size.

Table 1. Loads

Trial	Shear Force (lbs.)	Compressive Force (lbs.)	Force Ratio	L/D	LPS (Inches)
31	100	0	0	10	.015
32	100	124	1.24	10	.015
33	100	167	1.67	10	.015
43	125	0	0	5	.020
44	125	247	1.96	5	.020
45	125	33	2.97	5	.020
51	150	0	0	3.3	.025
52	150	183	1.22	3.3	.025
53	150	340	2.26	3.3	.025

Recording Data

Departing from the traditional graphic and photographic methods of recording photoelastic data, a fast and accurate system was developed for this investigation. The Shear Difference Method of calculating normal stresses requires data at a series of points on three parallel sections across the model. With some prior knowledge of the expected fringe pattern, (shown in Figures 15 and 16) these points can be laid out on tissue paper and placed over the model image on the polariscope screen. Using Tardy's method of compensation and a monochromatic filter to sharpen the fringes, the fringe order at each point may be determined accurately to at least one-hundredth of a fringe order. The isoclinic parameter at a point is determined by rotating the analyzer and polarizer to find the isoclinic that passes through that point. The isoclinic and isochromatic parameters may be fed into a computer and computed with the proper program with no further manipulation (Appendix I).

Traditional methods of recording data involve time-consuming and inaccurate tracing of fringe patterns and isoclinics, drawing curves of these parameters and interpolation from these curves.

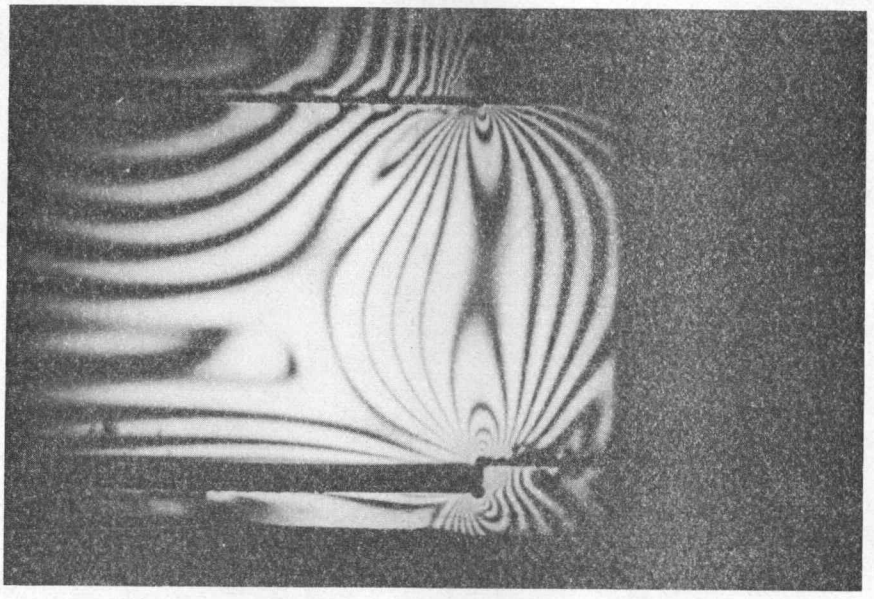

Figure 15. Isochromatic patterns - shear only.

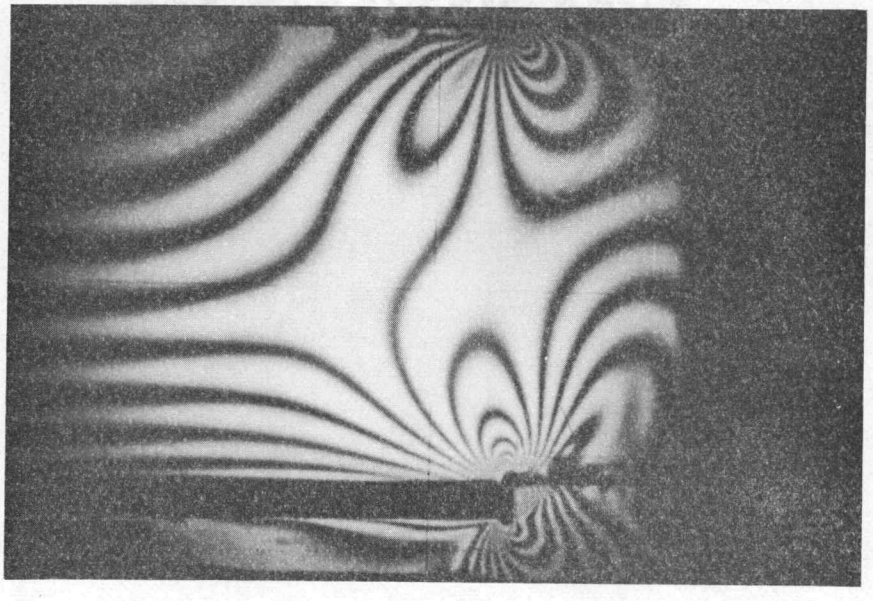

Figure 16. Isochromatic patterns - shear and axial.

Static Checks

Using static checks, the error of the curves associated with Equations (25) and (26) is established. In this investigation, a static check involves integrating the area under a curve (e.g. shear stress) and determining what force it represents. The integration is accomplished by determining the area under the curve with a polar planimeter and dividing by the length of the curve's base, and multiplying by the unit scale on the vertical axis. Then, multiplying by the cross sectional area yields the force. The difference between this force and the applied force, divided by the applied force, constitutes the error of the curve.

Fringe Value Determination

Because of the excessive creep in CR-39, determination of the fringe value under actual test conditions is advisable. The shear stress curve may be used for this purpose. This allows the fringe value to be found and the photoelastic analysis to proceed without delay rather than performing preliminary tests to establish the fringe value and then embark on the actual analysis.

The shear stress distribution is plotted and its average stress (τ_{ave}) calculated by means of a static check. The actual average shear stress (τ_{act}) is calculated knowing the applied shear force and

cross-sectional area of the beam.

A graph of the two average shear stresses τ_{act} and τ_{ave}, and the actual shear stress distribution are shown in Figure 17. It is assumed that the curve is of the correct profile, but not in the correct position with respect to the Y axis. Therefore, if the average of the experimentally determined curve coincides with the average of the actual shear stress, the curve will represent the shear stress distribution. Point A, Figure 17, is the average of the curve of the experimentally determined shear stress. If it is moved to B, the above condition will be met.

The stress at A can be calculated from Equation (25)

$$\tau_{ave} = n_y F_i \sin 2\theta$$

where F_i is some initial fringe value taken from literature. For A to coincide with B,

$$\tau_{ave} = \tau_{act}$$

Finding n_y and θ_y (Figure 17) by interpolation from the photoelastic data, the correct value becomes

$$F = \frac{\tau_{act}}{n_y \sin 2\theta_y} \quad .$$

This fringe value may be verified by performing the same calculation on the other point of average shear stress, C in Figure 17.

After several trials, F will be established for an approximate load and there will be no need to repeat this procedure for subsequent calculations.

The fringe value was determined initially by placing a CR-39 specimen in a tensile tester and calculating the fringe value in the usual manner. These results were very close to those obtained by the self-calibrating method.

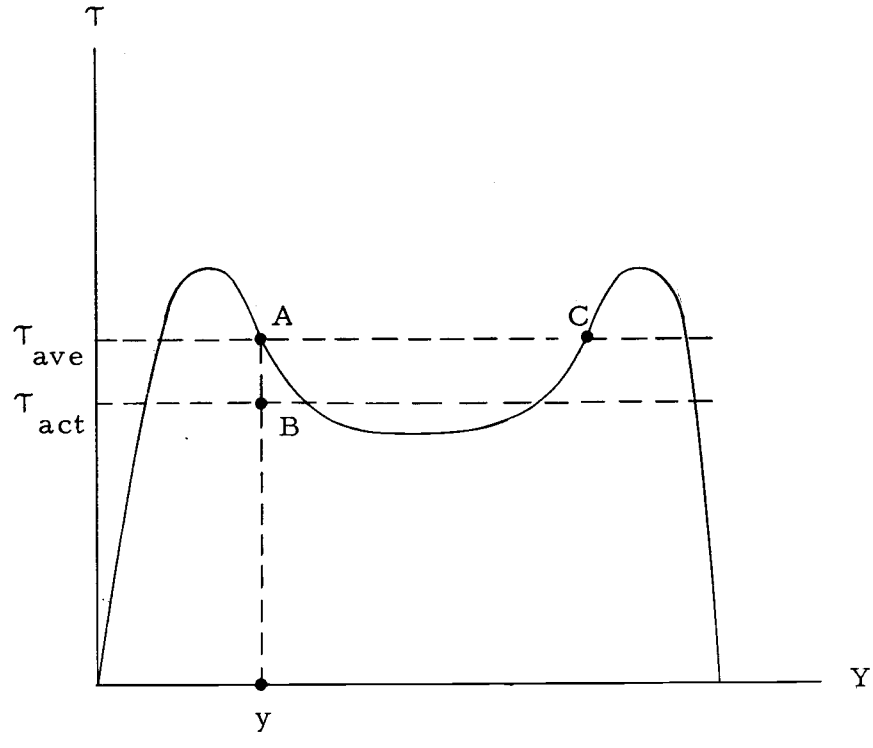

Figure 17. Fringe value determination.

VI. DATA REDUCTION

Shear Difference Method

The equations of equilibrium (8, vol. 1, p. 262)

$$\frac{\partial \sigma_x}{\partial x} + \frac{\partial \tau_{xy}}{\partial y} = 0$$

$$\frac{\partial \sigma_y}{\partial y} + \frac{\partial \tau_{xy}}{\partial x} = 0$$

are the basis for determining the normal stresses σ_x and σ_y across a straight section such as OY, Figure 18.

From the above,

$$(\sigma_y)_P = (\sigma_y)_O - \int_O^P \frac{\partial \tau_{xy}}{\partial x}\, dy \qquad (22)$$

where P and O denote points on Figure 18 and $(\sigma_y)_P$ and $(\sigma_y)_O$ are the stresses at those points.

Taking a section X-X through P parallel to the X axis and plotting the shear stress for that section, $\partial \tau_{xy}/\partial y$ at point P represents the slope with respect to the X axis of the shear stress curve at P' (Figure 18). The first approximation of the slope of the shear stress curve at P' is obtained by calculating the shear stress at P and an adjacent point A lying on the section X-X, and dividing their difference by the distance between them.

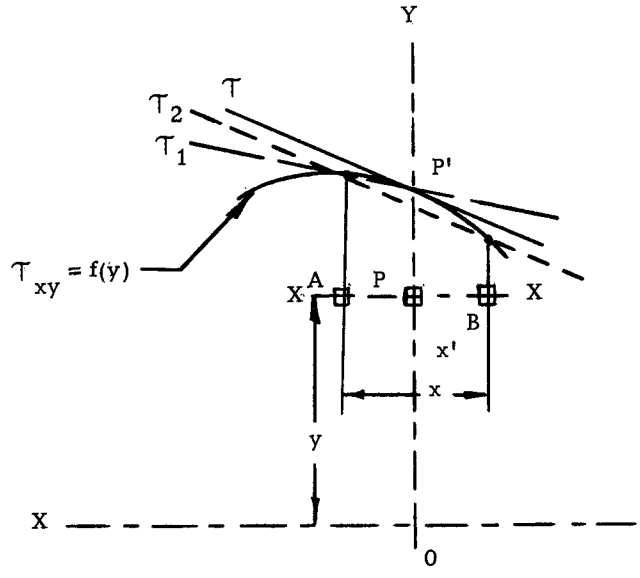

Figure 18. Shear difference method.

Then

$$\frac{\partial \tau_{xy}}{\partial x} = \frac{(\tau_{xy})_P - (\tau_{xy})_A}{\Delta x'} \tag{23}$$

In Figure 18, τ denotes the tangent to the shear curve at P', and τ_1 denotes the first approximation, Equation (23).

A second approximation can be obtained by taking the shear stress difference between the shears at two points, A and B, on opposite sides of P and on section X-X, and dividing by the distance between them.

This slope represented by τ_2 in Figure 18, is seen to be a better approximation to τ than τ_1. Thus

$$\frac{\partial \tau}{\partial x} = \frac{(\tau_{xy})_A - (\tau_{xy})_B}{\Delta x} \tag{24}$$

Substituting this into Equation (22),

$$(\sigma_y)_P = (\sigma_y)_O - (\Delta \tau_{xy}) \frac{\Delta y}{\Delta x}$$

or

$$(\sigma_y)_P = (\sigma_y)_O - \Delta \tau_{xy} C \tag{22a}$$

where

$$C = \frac{\Delta y}{\Delta x}$$

Applying this method in a step-wise fashion across a section, a profile of the normal stress is obtained.

The shear stress (5, p. 184) at each point is calculated using photoelastic data and is given by

$$\tau_{xy} = nF \sin 2\theta \tag{25}$$

The stress parallel to the X axis can be derived from Mohr's circle. From Figure 19,

$$d = \tau_{max} \cos 2\theta$$

and

$$\sigma_x = \sigma_y - 2\tau_{max} \cos 2\theta$$

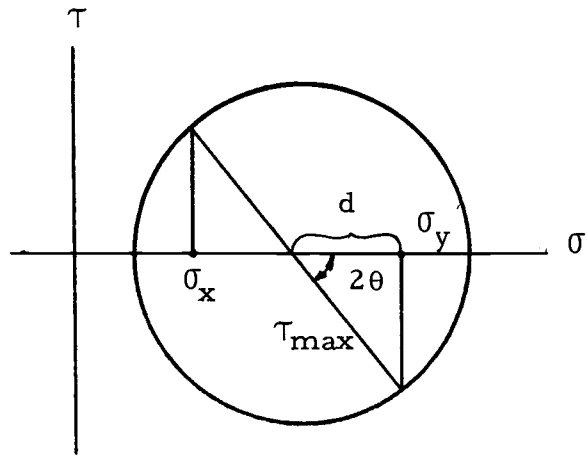

Figure 19. Mohr's Circle.

since,

$$\tau_{max} = nF \tag{21}$$

$$\sigma_x = \sigma_y - 2nF \cos 2\theta \tag{26}$$

Figure 20 shows the Cartesian coordinate system used in this analysis. The origin, O, is located on the edge of the model under the load as indicated; and sections one and two, adjacent to the plane of investigation, are the sections on which the shear stress is determined for calculating the shear stress difference (Equation 25). The digital computer program written for solving Equations (25), (22a) and (26) and calculating the octahedral shear stress is shown in Appendix I.

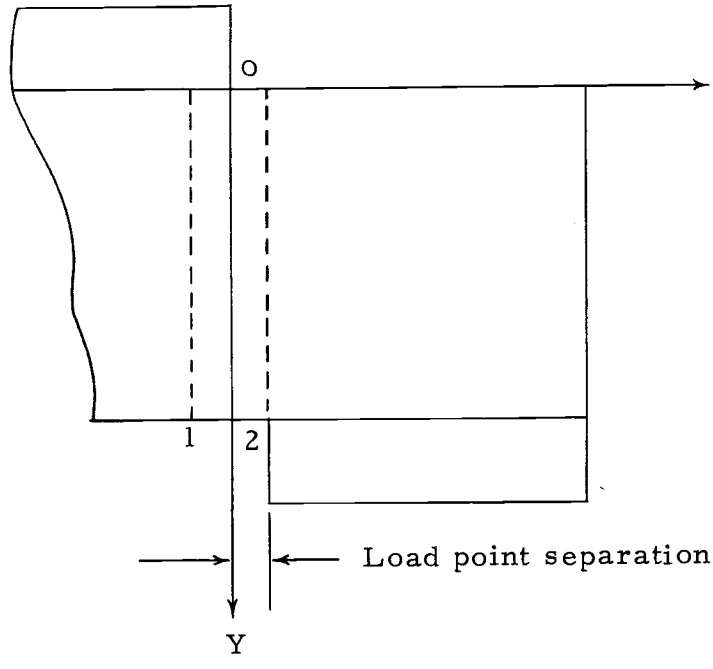

Figure 20. Cartesian coordinate system.

VII. RESULTS AND CONCLUSIONS

Octahedral Shear Stress

Using the principal stresses determined from the photoelastic analysis, the octahedral shear stress at selected points along the section of interest (section A-A, Figure 1) can be calculated. The results for each point is plotted on a coordinate axis system having the ratio of coordinate distance Y (Figure 20) to the depth of the model D (Figure 14) on the abscissa, and the octahedral shear stress on the ordinate.

The octahedral shear stress for trial 4 is shown in Figure 21 with results of trials 3 and 5 appearing in Figure 22. Trial 4 is used as an example because the stress ratios (Table I) are the greatest and best display the increased octahedral shear stress.

From Figure 21, it is apparent that the octahedral shear stress increases as the axial compression increases. In view of the principles of failure outlined in Chapter II, it is concluded that a beam loaded in shear will approach failure as axial compression is applied.

The curves in Figure 21 and Figure 22 indicate that the greatest increase in octahedral shear stress occurs under the load point near the top of the beam.

As discussed in Chapter II, the approach of failure of an individual point may also be plotted (Figure 7) as a function of the principal

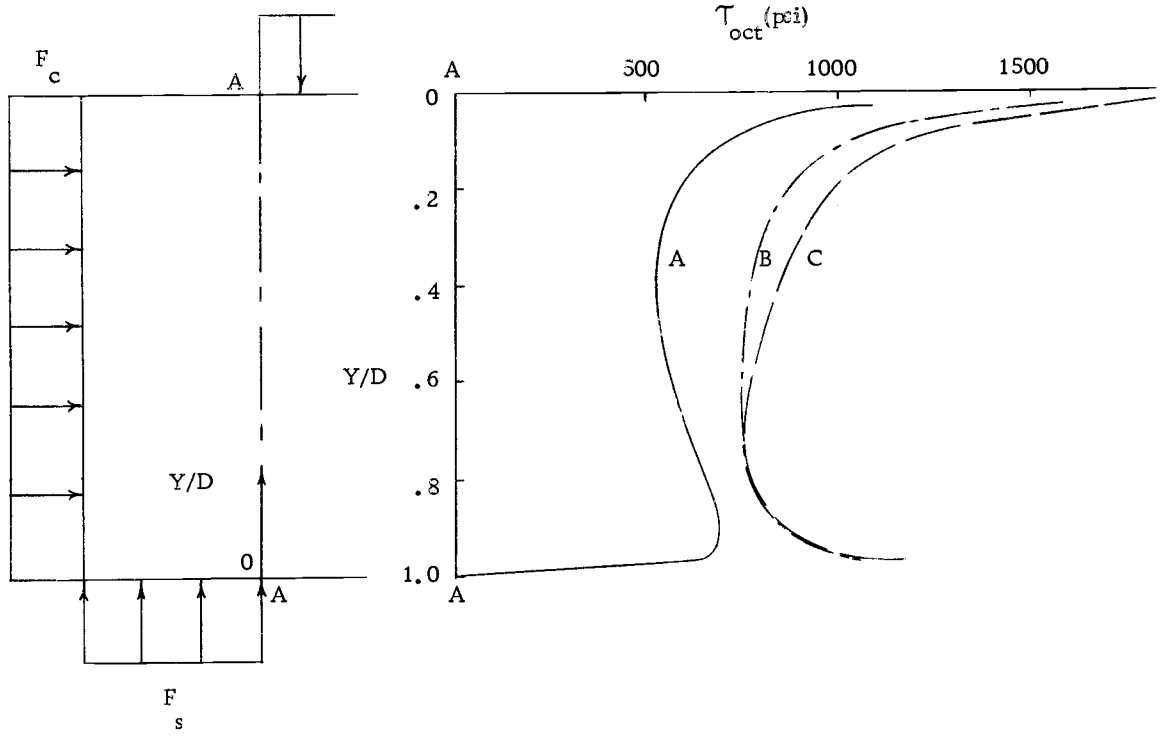

Curve	Trial	Shear Force	Compressive Force
A	43	F_s = 125 lb	F_c = 0 lb
B	44	F_s = 125 lb	F_c = 247 lb
C	45	F_s = 125 lb	F_c = 331 lb

Beam dimensions: 1/4 x 3/4 x 2-1/2 in.

Figure 21. Octahedral shear stress - trial 4.

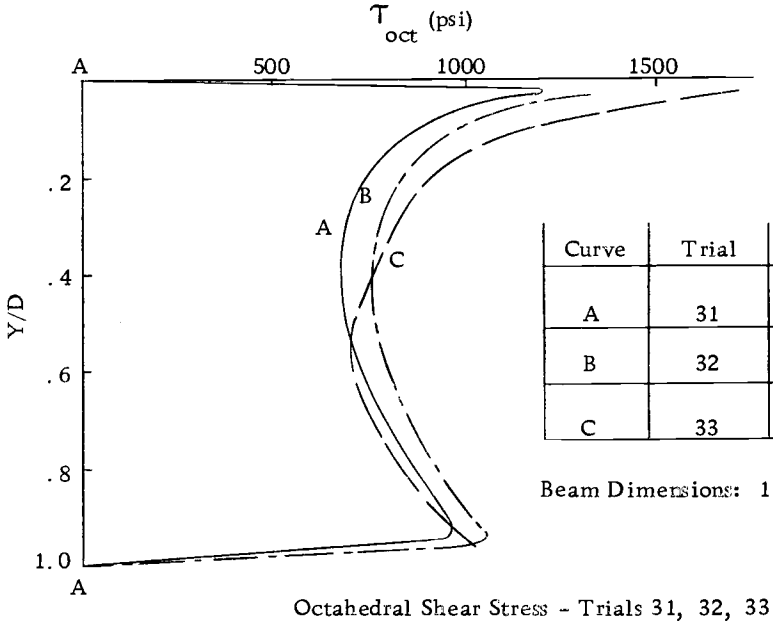

Curve	Trial	Shear Force	Compr. Force
A	31	100 lb.	0 lb.
B	32	100 lb.	129 lb.
C	33	100 lb.	167 lb.

Beam Dimensions: 1/4 x 1/2 x 2-1/2 in.

Octahedral Shear Stress - Trials 31, 32, 33

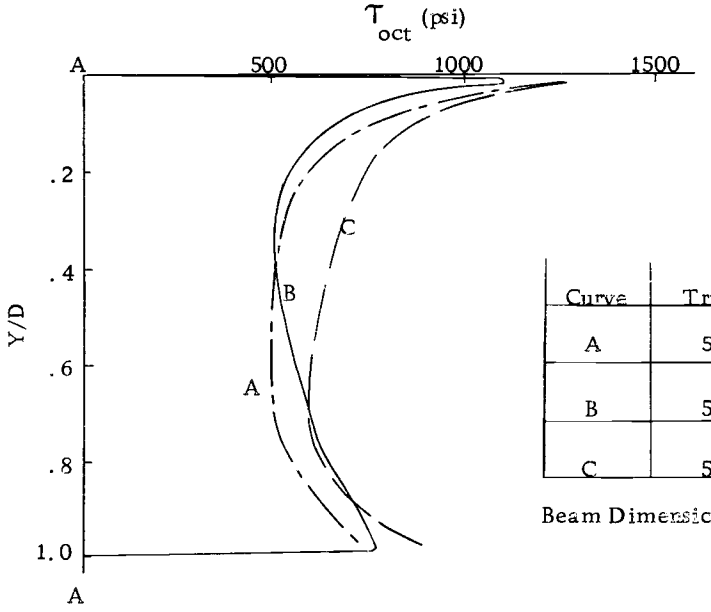

Curve	Trial	Shear Force	Compr. Force
A	51	150 lb.	0 lb.
B	52	150 lb.	183 lb.
C	53	150 lb.	340 lb.

Beam Dimensions 1/4 x 1 x 2-1/2 in.

Octahedral Shear Stress - Trials 51, 52, 53

Figure 22. Octahedral shear stress - trials 3 and 5.

stresses. Figure 23 shows the principal stresses for point Y/D = .20 and .50 in Trial 4. The points A, B, and C represent the principal stresses as the axial force is increased. It is seen that the points approach the elliptical boundary (in this case arbitrarily placed) and that if the test were continued to failure, the line ABC would intersect the boundary (hypothetically) at D indicating that the yield point had been reached and failure will ensue.

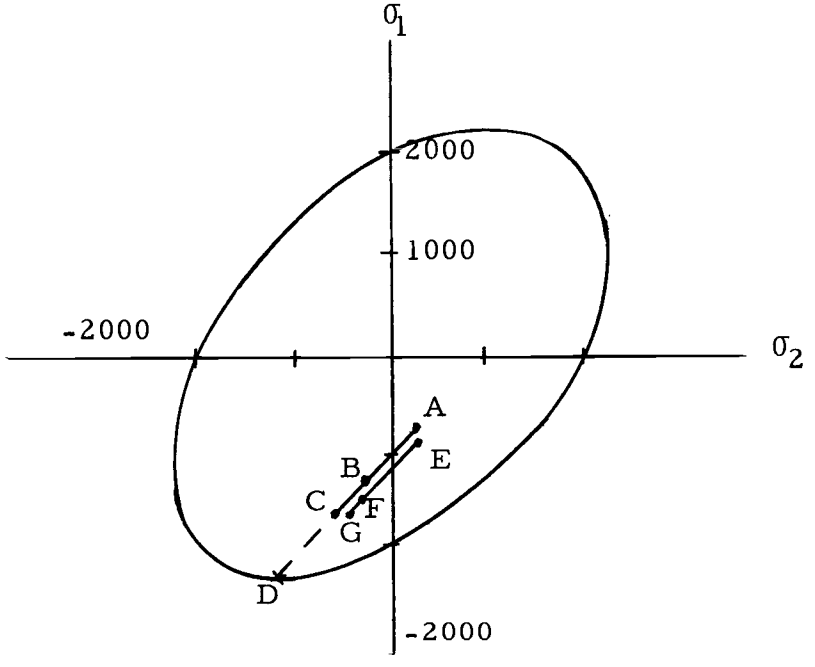

Figure 23. Distortion energy failure criteria - trial 4.

Normal Stresses

As stated in the Chapter I, it is a preliminary objective of this investigation to photoelastically determine the normal stresses at section A-A, Figure 1. The normal stresses, as calculated from the photoelastic data using the computer program (Appendix I), are

displayed as curves plotted on an abscissa of the ratio of Y/D described previously.

The results of Trial 3 are plotted in Figure 24 while those of Trials 4 and 5 are shown in Figure 25.

The shear stress curve for Trial 31 (top figure, Figure 24) is very much like that cited by Coker and Filon as described in Chapter I, in which the maximum stress occurs near the edges of the beam.

The application of axial compression reduces the peak shear stress near the edges somewhat and increases the stress in the central portion of the beam. Since the area under the shear stress must remain constant for a given shear load even though axial compression is added, the change in the shear stress can only be refected in a redistribution of the area about the line of average shear stress.

The σ_x profile indicates that the model is in compression near the edges and in tension in the midsection. This is substantially the same results obtained by Goodier in his analysis of a block compressed by two concentrated forces.

The error of the σ_x curve is determined with a polar planimeter as described in Chapter V. In Trial 31, Figure 24, where there is no axial force, the area above the abscissa must equal that below the abscissa or static equilibrium will not be maintained.

As axial compression is applied, Trials 32 and 33, Figure 24, it is superimposed on the σ_x profile of Trial 31. This is apparent since the

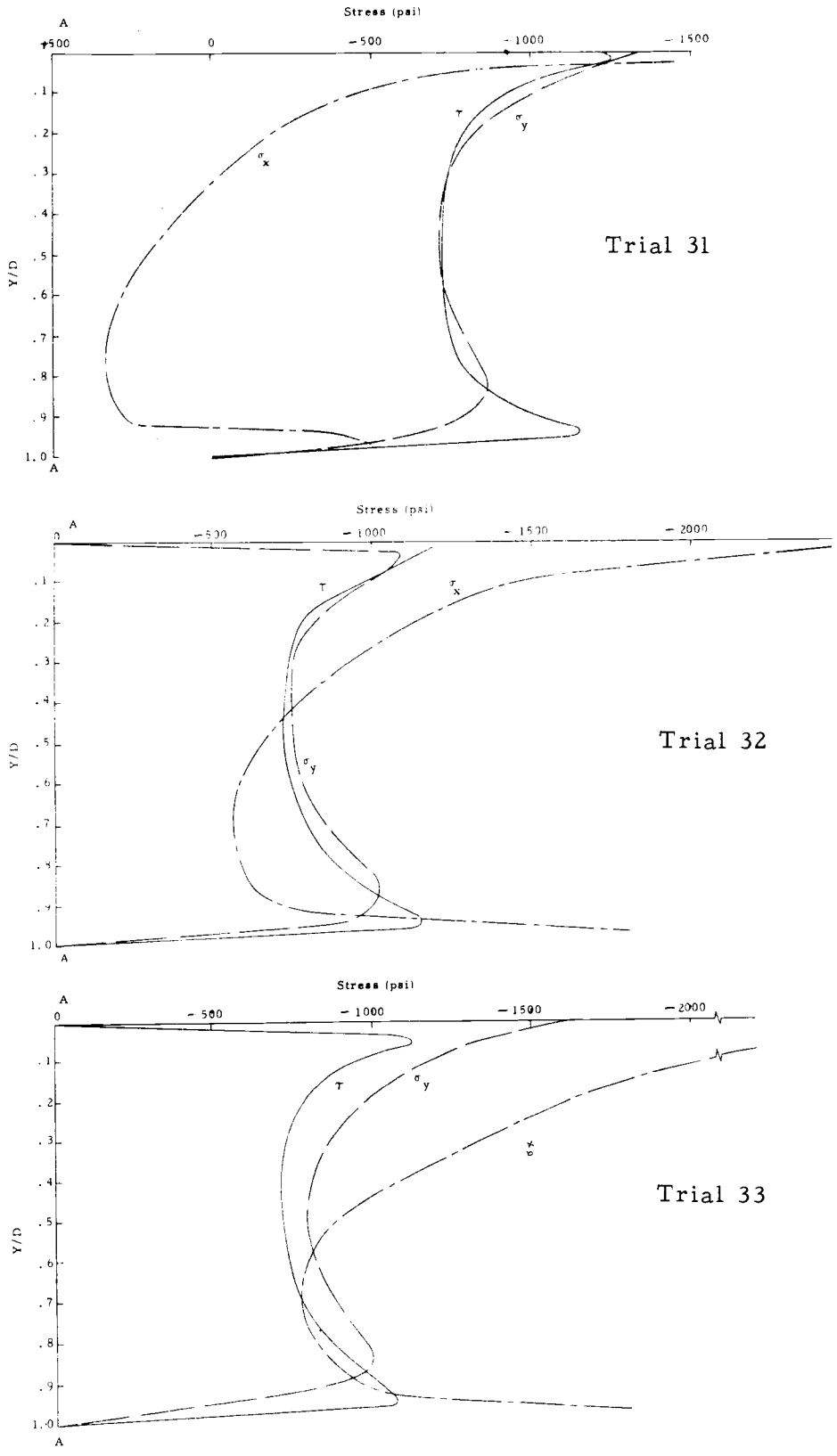

Figure 24. Shear and normal stress distribution at shear plane A-A Trial 3

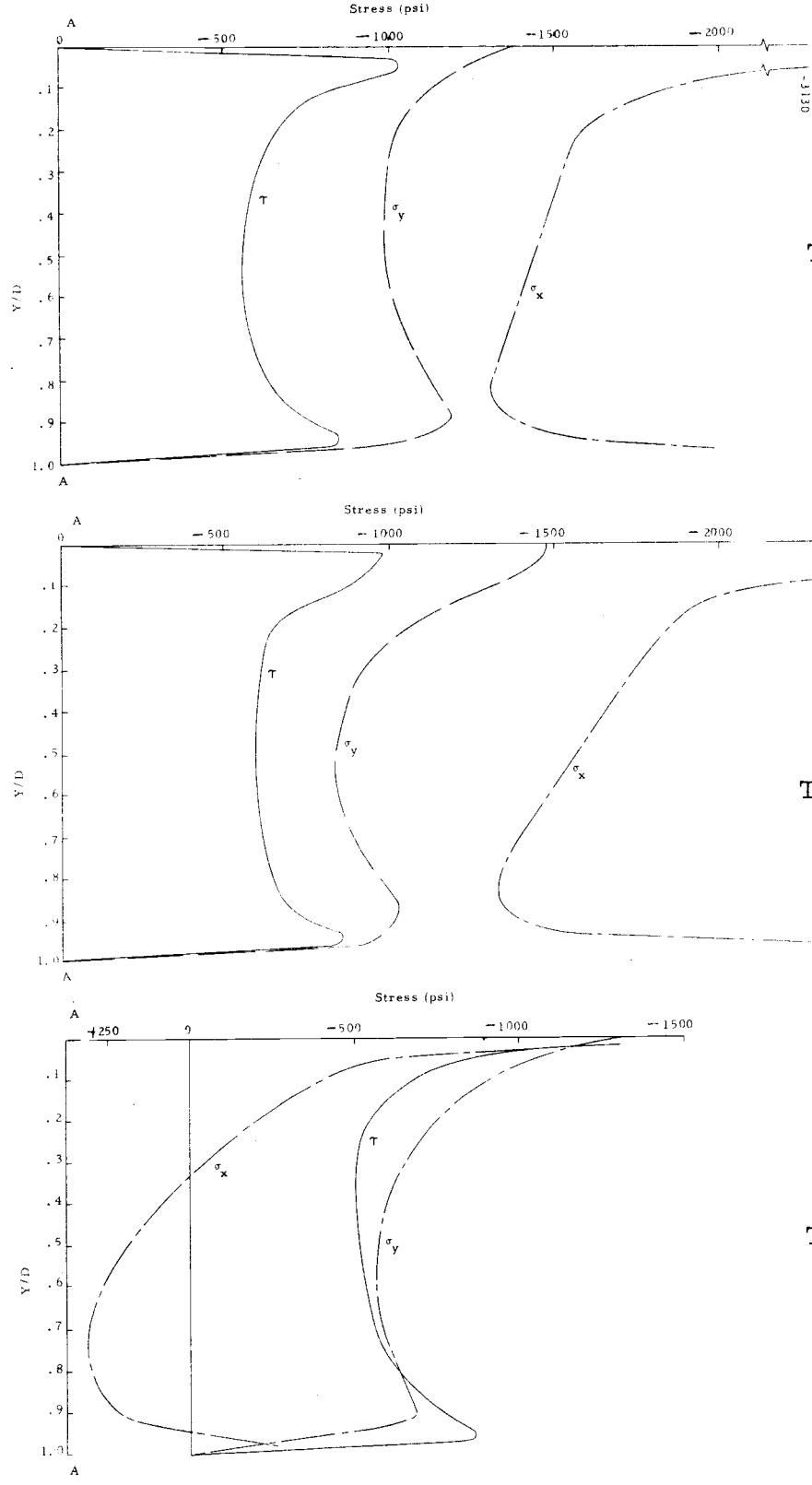

Figure 25. Shear and normal stress distribution at shear plane A-A Trials 4 and 5

profile is approximately the same for all three trials; only the position with respect to the abscissa changes.

The σ_y profile is similar in shape and magnitude to the shear stress curve. It is not affected much by axial compression except at higher axial loads where the increase in σ_y is due primarily to the poisson effect. It is not possible to check the error of the σ_y curve using a static check. The only way of verifying the curve is by the fact that there is no load on the bottom of section A-A, Figure 1. Therefore, the σ_y curve must approach zero near $Y/D = 1.0$. In the region of the origin, the σ_y curve should be approximately equal to the boundary condition $(\sigma_y)_O$. In actuality, if the σ_x curves prove satisfactory by a static check then the σ_y curve must be correct because they are dependent upon one another.

Experimental Error

The percent error of these curves is generally in the range of 1.5% to 2.0%, as determined by means of a static check (see Chapter V).

Although steps were taken to compensate for optical creep, it can not be eliminated completely in cases where the photoelastic data is recorded over a length of time. The fringe value may change from one side of the beam during the recording of data to another due to optical creep. For this reason, the self-calibration technique used

in this investigation will yield average values.

On several occasions, the stress created at points in the model were in the area of 3000 psi. As discussed in Chapter IV, this is the region where the stress-strain relationship starts to become non-linear and the accuracy of photoelasticity decreases.

The stress pattern in the model under high axial compression becomes quite complicated (Figure 16) and it is difficult to determine the fringe order.

VIII. RECOMMENDATIONS

It is recommended that further investigations be conducted using a wider range of beam dimensions (L/D) and force ratios (F_c/F_s) to better establish the effect of combined shear and axial compression on a shear plane.

If greater force ratios are to be used, another method of applying the axial compression will have to be found. It is the opinion of the author that the compression assembly (Figure 10) developed for this investigation was employed to its capacity and can not be used to achieve greater loads with acceptable reliability.

Some bending may be present due to the method used to apply the shear load. These effects could be minimized by confining the top edges of the beam as was done by Fukuda (Figure 2).

It would be of great interest to conduct these tests to failure to varify the conclusions reached in this investigation and to study the mode of failure. This area might well be investigated employing photoelasticity.

BIBLIOGRAPHY

1. Coker, E. G. and L. N. G. Filon. A treatise on photo-elasticity. Cambridge, Eng., Cambridge University, 1931. 720 p.

2. Coolidge, D. J. An investigation of the mechanical and stress-optical properties of Columbia Resin, CR-39. Proceedings of the Society for Experimental Stress Analysis 6(1): 74-82. 1948.

3. Durant, M. J. and F. Garwood. Stress in a deep beam. Ministry of Works Technical Note No. 78. London. Oct. 1947.

4. Durelli, A. J. Distribution of stresses in partial compression and a new method of determining the isostatics in photoelasticity. In: Proceedings of the thirteenth Semi-Annual Eastern Photoelasticity Conference, Cambridge, Mass., 1941. Cambridge, (1941) p. 25.

5. Durelli, A. J. and W. F. Riley. Introduction to photomechanics. Englewood Cliff, N. J., Prentice-Hall, 1965. 402 p.

6. Filon, L. N. G. A Manual of photo-elasticity for engineers. London, Cambridge University, 1936. 140 p.

7. Filon, L. N. G. On an approximate solution for the bending of a beam of rectangular cross-section under any system of load, with specific reference to points of concentrated or discontinuous loading. Philosophical Transactions of the Royal Society (London), ser. A, 201:63-155.

8. Frocht, Max Mark. Photoelasticity. New York, John Wiley, 1941, 2 vol.

9. Goodier, J. N. Compression of rectangular blocks and the bending of beams by non-linear distribution of bending forces. Transactions of the American Society of Mechanical Engineers, Applied Mechanics 54: 173-183. 1932.

10. Haigh, B. P. The strain energy function and the elastic limit. Engineering 109: 158-160. Jan. 30, 1920.

11. Hurlock, Les. Strain gage measurement concepts. Beaverton, Oregon, Tektronix, 1966. 66 p.

12. Norris, C. B. Strength of orthotropic materials subjected to combined stresses. U. S. Forest Products Laboratory Report 1816. Madison, Wis. 1962.

13. Seely, Fred B. and James O. Smith. Advanced Mechanics of Materials. New York, John Wiley, 1952. 680 p.

14. Singer, Ferdinand L. Strength of materials. 2nd ed. New York, Harper, 1951. 469 p.

15. Timoshenko, S. Strength of materials. Part II. New York, Van Nostrand, 1966. 572 p.

16. Timoshenko, S. and J. N. Goodier. Theory of elasticity. 2nd ed. New York, McGraw-Hill, 1951. 506 p.

APPENDIX

APPENDIX I

Shear Difference Method
Computer Program

DECEMBER 3, 1969 11:22 AM TERMINAL 033

#EDIT

]FIN, PHOTOEL

]

LIST

```
00001:          PROGRAM PHOTOEL
00002:          REAL, N, N1, N2
00003:          WRITE(61, 9)
00004:9         FORMAT('SHEAR DIFFERENCE METHOD')
00005:          WRITE(61, 10)
00006:10        FORMAT('SUBSCRIPTS 1 AND 2 REFER TO SECTION ADJACENT')
00007:          WRITE961, 11)
00008:11        FORMAT('TO SECTION TO BE ANALYZED')
00009           WRITE(61, 12)
00010:12        FORMAT('N IS THE FRINGE ORDER, F IS THE FRINGE VALUE')
00011:          WRITE(61, 13)
00012:13        FORMAT('C IS DX/DY, SIGMAY IS BOUNDARY CONDITION')
00013:          F = TITYIN(3HF=)
00014:          SIGMAY = TITYIN(4HSIGM, 4HAY =)
00015:          WRITE(61, 14)
00016:14        FORMAT('YD       SIGMAX    SIGMAY       P          Q          TAU      T'

00017:         1'AUMAX TAUOCT')
00018:5         READ(35, 1) YD, N, N1, N2, THETA1, THETA2, C
00019:1         FORMAT(F5.3, 3F6.2, 3F5.1, F5.3)
00020:          IF(N) 8, 8, 2
00021:2         TAU=F*N*SIN(2.0*THETA*.01745)
00022:          TAU1=F*N1*SIN(2.0*THETA*.01745)
00023:          TAU2=F*N2*SIN(2.0*THETA*.01745)
00024:          DELTAU=TAU1-TAU2
00025:          DTAU=C*DELTAU
00026:          SIGMAY=SIGMAY-DTAU
00027:          A=2.0*N*F*COS(2.0*THETA*.01745)
00028:          IF(THETA-45) 3, 3, 6
00029:3         SIGMAX=SIGMAY+ABS(A)
00030           GO TO 7
00031:6         SIGMAX=SIGMAY-ABS(A)
00032:          GO TO 7
00033:7         TAUMAX=N*F
00034:          G=(SIGMAX+SIGMAY)/2.0
00035:          P=G+TAUMAX
00036:          Q=G-TAUMAX
00037:          TAUOCT=(SORT(((P-Q)**2)+((ABS(P)**2)+((ABS(Q))**2)))/3.0

00038:          WRITE(61, 4) YD, SIGMAX, SIGMAY, P, Q, TAU, TAUMAX, TAUOCT
00039:4         FORMAT(' ', F5.3, 7F.0)
00040:          GO TO 5
```

```
00041:8         STOP
00042:          END

]
```